SUBSURFACE WATER ICE MAPPING (SWIM) ON MARS: GEOMORPHIC MAPPING. D.M.H. Baker[1], G.A. Morgan[2], R.H. Hoover[3], A. Pathare[2], C.M. Dundas[4], N.E. Putzig[2], and the SWIM Team. [1]NASA Goddard Space Flight Center (david.m.hollibaughbaker@nasa.gov), [2]Planetary Science Institute, [3]Southwest Research Institute, [4]U.S. Geological Survey.

Introduction: The Subsurface Water Ice Mapping (SWIM) project supports an effort by NASA's Mars Exploration Program to determine *in situ* resource availability [1-2]. We are performing global reconnaissance mapping as well as focused multi-dataset mapping to characterize the distribution of water ice from 60ºS to 60ºN latitude. In 2019, we produced ice consistency maps for the northern hemisphere (0–60ºN) from 0–225ºE and 290–360ºE longitude. In 2020, we are extending our mapping into the southern hemisphere (0–60ºS) and from 225–290ºE longitude in the northern hemisphere at elevations <+1km. Our maps are being made available on the SWIM Project website (https://swim.psi.edu), and we intend to complete our global mapping by the summer of 2020. Follow us on Twitter @RedPlanetSWIM for project news and product release information.

The SWIM Datasets: To search for and assess the presence of shallow ice across our study regions, we are integrating multiple datasets to provide a holistic view of the upper 10s of m of the Martian subsurface. The individual datasets and methods we employ include neutron-detected hydrogen maps (MONS), thermal behavior (TES, THEMIS, and MCS), multiscale geomorphology (HiRISE, CTX, HRSC, and MOLA), and SHARAD surface and subsurface radar echoes.

Consistency Mapping: For the SWIM 2019 maps, we used the SWIM equation [2-3] to provide a quantitative assessment of how consistent (or inconsistent) the various remote sensing datasets are with the presence of shallow (<5 m) ice. The SWIM Equation yields values ranging between +1 and -1, where +1 means that all of the data are consistent with the presence of ice, 0 means that the data give no indications of the presence or absence of ice, and -1 means that the data are inconsistent with the presence of ice. Here, we focus on ice consistency values from geomorphic mapping.

For more information on the project and its techniques and datasets, visit our website and associated presentations at this LPSC: Putzig et al. (summary of results), Perry et al. (SWIM Equation and methods), Sizemore et al. (thermal and neutron analysis), Morgan et al. (radar surface reflectivity), Petersen et al. (radar subsurface mapping), and Bain et al. (focused regions).

SWIM 2019 Methods: The SWIM 2019 geomorphology ice consistency map [1,2,4] (**Fig. 1**) was based on previous and new mapping of the presence of periglacial and glacial landforms inferred to have required ice for their genesis. A sampling of 4x4° CTX image mosaics (beta01 versions from the Caltech Murray Lab [5]) within previously mapped geologic units [6] was used to tally the number of observed periglacial and glacial landforms and to extrapolate the observations to the geologic unit boundaries. The number of landforms was then normalized with equal weighting to yield ice consistency values between 0 and 1. Areas <27°N with no periglacial or glacial features were assigned a value of -1 and areas from 30° to 27°N were assigned an equatorward Gaussian decay in values from 0.1 to 0. Areas of scalloped terrain in Acidalia (0-70°W) were assigned a value of 0.75. Previous mapping was also used, including glacial features (lobate debris aprons, lineated valley fill, and concentric crater fill; [7])

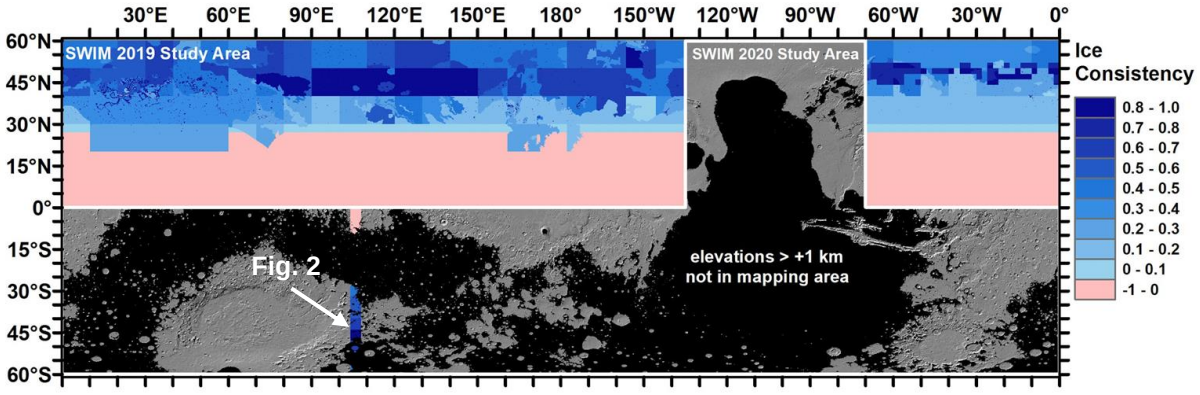

Fig. 1. SWIM project study regions and results for geomorphology ice consistency mapping. Ice consistency values [1-3] are indicated for the northern hemisphere SWIM 2019 study and preliminary work for SWIM 2020.

and pedestal craters [8]; glacial features were assigned a value of 1 and pedestal craters a value of 0.75.

SWIM 2019 Results: Our SWIM 2019 results from the northern hemisphere (**Fig. 1**) show that periglacial and glacial landforms are widespread and are concentrated in the 40–50°N latitude band (i.e., areas of highest ice consistency values) and within specific regions, including Arcadia and Utopia Planitiae and Deuteronilus Mensae. There is also a paucity of periglacial and glacial landforms equatorward of ~30°N, with the exception of some mantling units and glacial landforms near Deuteronilus Mensae (10–60°E) and Arcadia Planitia (160–190°E). This equatorward limit is consistent with previous mapping from individual images [e.g., 10]. The lack of higher-latitude features leading to lower consistency values may indicate that ice-related geomorphology is less diverse there, possibly because some of the features indicate partial ice loss.

SWIM 2020 Methods: Following the SWIM 2019 grid mapping methods [9], we are in the process of mapping the occurrence of periglacial and glacial landforms in the southern hemisphere and areas north of the Tharsis region (**Fig. 1**). As an enhancement to our previous mapping approach, we are planning to complete surveying at a preliminary grid cell size of 4x4°, tied to the CTX mosaic quads. We plan to increase the mapping resolution to 1x1° in the 30–40° latitude range to better define the equatorward boundary of ice-rich landforms.

Preliminary Results: A longitudinal strip of 4x4° CTX mosaic quads was surveyed as a preliminary assessment of the types and locations of landforms expected within the study region. Like the northern hemisphere, ice-rich landforms are generally absent equatorward of about 30°S [10], with the exception of intracrater materials resembling degraded concentric crater fill. Lobate debris aprons and pedestal craters are common, and textured mantling units are widespread with various degrees of pitting (**Fig. 2**).

Revised Consistency Mapping: We are currently revisiting the methods of assigning geomorphology ice consistency values for input to the SWIM equation [3]. A more quantitative approach is to use Bayesian statistics with probability density functions describing the ice content for each geomorphic landform. Although this is challenging due to the complexity of interpreting the origin and evolution of some landforms, a generalized approach is to use published models and observations to constrain the ice content necessary for formation. For example, current numerical models of scalloped depressions in Utopia require an ice content of the unit in which they occur to be nearly pure (>90%) ice [11]. Most glacial features (LDA, LVF, CCF) are highly likely to contain >80% ice based on regional SHARAD radar surveys [12] and probably contain at least 40% ice based on rheological models [13]. Landforms with more uncertain ice contents (e.g., mantling units) may necessitate a large range of probable values with equal weighting. We will continue to refine the assignment of ice probability values in future work. We hope to provide a more rigorous basis for assigning ice consistency values than was achieved previously for SWIM 2019.

Future Work: We will present more complete maps of the distribution of observed periglacial and glacial landforms within the study region, including their inferred consistency with the presence of subsurface ice. We also plan to complete detailed descriptions of periglacial and glacial landforms proximal to icy craters and scarps [14,15]. This will enable us to check the correlation of local areas of known near-surface ice to regional landform mapping and ice consistency values.

Acknowledgments: The SWIM project is supported by NASA through JPL Subcontracts 1611855/1639821. Thanks to the Caltech Murray Lab for making the CTX mosaics publicly available (http://murray-lab.caltech.edu/CTX/).

References: [1] Morgan, G.A. et al., Mapping Water Ice on Mars: Human Mission Resources and Climatic Implications, submitted to *Nature Astronomy*. [2] Putzig, N.E. et al. (2019) *Ninth Int. Conf. Mars*, 6427. [3] Perry, M.R. et al. (2019) *LPSC 50*, 3083. [4] Putzig, N.E. et al. (2019) *LPSC 50*, 2087. [5] Dickson, J.L. et al. (2018) *LPSC 49*, 2480. [6] Tanaka, K.L. et al. (2005) *USGS SIM 2888*. [7] Levy J. et al. (2014) *JGR* 119, 2188–2196. [8] Kadish, S.J. et al. (2009) *JGR* 114, E10001. [9] Ramsdale, J.D. et al. (2017) *PSS* 140, 49–61. [10] Milliken R.E. et al. (2003) *JGR* 108, E6, 5057. [11] Dundas, C.M. et al. (2015) *Icarus* 262, 154–169. [12] Petersen, E.I. et al. (2018) *GRL* 45, 11,595–11,604. [13] Li, H. et al. (2005) *Icarus* 2, 382–394. [14] Dundas, C.M. et al. (2014) *JGR* 119, 109–127. [15] Dundas C.M. et al. (2018) *Science*, 359, 199–201.

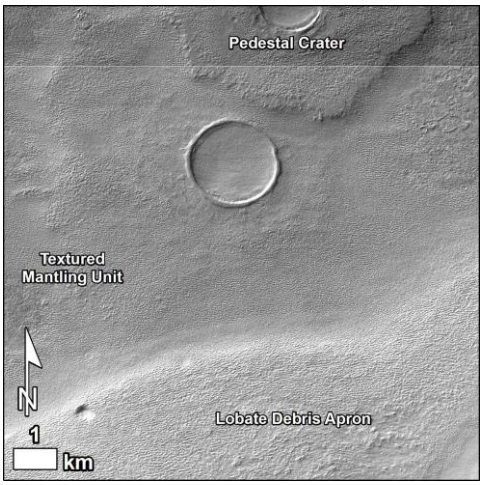

Fig. 2. Example of mapped landforms (CTX; 44.1°S, 107.5°E).